Analysis and experimental assessment of the sensitivity of stimulated Raman scattering microscopy

Yasuyuki Ozeki,[1,*] Fumihiro Dake,[1] Shin'ichiro Kajiyama,[2] Kiichi Fukui,[3] and Kazuyoshi Itoh[1]

[1] *Department of Material and Life Science,Graduate School of Engineering, Osaka University, 2-1 Yamadaoka, Suita, Osaka 565-0871, Japan*
[2] *School of Biology-Oriented Science and Technology, Kinki University, 930 Nishimitani, Kinokawa, Wakayama 649-6493, Japan*
[3] *Department of Biotechnology,Graduate School of Engineering, Osaka University, 2-1 Yamadaoka, Suita, Osaka 565-0871, Japan*
[*] *Corresponding author: ozeki@mls.eng.osaka-u.ac.jp*

Abstract: We theoretically show that the shot-noise-limited sensitivity of stimulated Raman scattering (SRS) microscopy, which enables high-contrast vibrational imaging, is similar to that of coherent anti-Stokes Raman scattering microscopy. We experimentally confirm that the sensitivity of our SRS microscope is lower than the shot-noise limit only by <15 dB, which indicates that the high-sensitivity of SRS microscopy is readily available.

OCIS codes: (180.5655) Raman microscopy; (190.2640) Stimulated scattering, modulation, etc.; (300.6290) Spectroscopy, four-wave mixing; (180.6900) Three-dimensional microscopy; (190.4410) Nonlinear optics, parametric processes.

References and links

1. Y. Barad, H. Eisenberg, M. Horowitz, and Y. Silberberg, "Nonlinear scanning laser microscopy by third harmonic generation," Appl. Phys. Lett. **70**, 922-924 (1997).
2. P. J. Campagnola, M.-D. Wei, A. Lewis, and L. M. Loew, "High-resolution nonlinear optical imaging of live cells by second harmonic generation," Biophys. J. **77**, 3341-3349 (1999).
3. A. Zumbusch, G. R. Holtom, and X. S. Xie, "Three-dimensional vibrational imaging by coherent anti-Stokes Raman scattering," Phys. Rev. Lett. **82**, 4142-4145 (1999).
4. K. Isobe, S. Kataoka, R. Murase, W. Watanabe, T. Higashi, S. Kawakami, S. Matsunaga, K. Fukui, and K. Itoh, "Stimulated parametric emission microscopy," Opt. Express **14**, 786-793 (2006), http://www.opticsinfobase.org/abstract.cfm?URI=oe-14-2-786.
5. D. Fu, T. Ye, T. E. Matthews, G. Yurtsever, and W. S. Warren, "Two-color, two-photon, and excited-state absorption microscopy," J. Biomed. Opt. **12**, 054004 (2007).
6. C. L. Evans, E. O. Potma, M. Puoris'haag, D. Côté, C. P. Lin, and X. S. Xie, "Chemical imaging of tissue in vivo with video-rate coherent anti-Stokes Raman scattering microscopy," Proc. Natl. Acad. Sci. U.S.A. **102**, 16807-16812 (2005).
7. A. Volkmer, J.-X. Cheng, and X. S. Xie, "Vibrational imaging with high sensitivity via epidetected coherent anti-Stokes Raman scattering microscopy," Phys. Rev. Lett. **87**, 23901 (2001).
8. J. -X. Cheng, L. D. Book, and X. S. Xie, "Polarization coherent anti-Stokes Raman scattering microscopy," Opt. Lett. **26**, 1341-1343 (2001), http://www.opticsinfobase.org/abstract.cfm?URI=ol-26-17-1341.
9. C. L. Evans, E. O. Potma, and X. S. Xie, "Coherent anti-Stokes Raman scattering spectral interferometry: determination of the real and imaginary components of nonlinear susceptibility $\chi^{(3)}$ for vibrational microscopy," Opt. Lett. **29**, 2923-2925 (2004), http://www.opticsinfobase.org/ol/abstract.cfm?URI=ol-29-24-2923.
10. F. Ganikhanov, C. L. Evans, B. G. Saar, and X. S. Xie, "High-sensitivity vibrational imaging with frequency modulation coherent anti-Stokes Raman scattering (FM CARS) microscopy," Opt. Lett. **31**, 1872-1874 (2006), http://www.opticsinfobase.org/ol/abstract.cfm?URI=ol-31-12-1872.
11. H. Kano and H. Hamaguchi, "Vibrationally resonant imaging of a single living cell by supercontinuum-based multiplex coherent anti-Stokes Raman scattering microspectroscopy," Opt. Express **13**, 1322-1327 (2005), http://www.opticsinfobase.org/abstract.cfm?URI=oe-13-4-1322.
12. R. W. Boyd, *Nonlinear optics 2nd ed.* (Academic, 2003).

#106468 - $15.00 USD Received 16 Jan 2009; revised 21 Feb 2009; accepted 21 Feb 2009; published 24 Feb 2009

13. P. Nandakumar, A. Kovalev, and A. Volkmer, "Vibrational imaging and microspectroscopies based on coherent anti-Stokes Raman scattering microscopy," the 8th European/French Israeli Symposium on Nonlinear and Quantum Optics, Mo-B, 2005, http://www.weizmann.ac.il/conferences/frisno8/program.html.
14. E. Ploetz, S. Laimgruber, S. Berner, W. Zinth, and P. Gilch, "Femtosecond stimulated Raman microscopy," Appl. Phys. B **87**, 389-393 (2007).
15. F. Dake, Y. Ozeki, and K. Itoh, "Principle confirmation of stimulated Raman scattering microscopy," presented at Optics & Photonics Japan (OPJ2008), paper 5pC12, Tsukuba, Nov. 5th, 2008 (in Japanese).
16. C. W. Freudiger, W. Min, B. G. Saar, S. Lu, G. R. Holtom, C. He, J. C. Tsai, J. X. Kang, and X. S. Xie, "Label-free biomedical imaging with high sensitivity by stimulated Raman scattering microscopy," Science **322**, 1857-1861 (2008).
17. R. P. Feynman, R. B. Leighton, and M. Sands, *The Feynman lectures on physics* (Addison-Wesley, 1963).

1. Introduction

Coherent nonlinear-optical microscopy techniques [1-5], which exploit nonlinear-optical interactions induced by tightly focused laser pulses, have provided a way to three-dimensionally visualize unstained biological samples. In particular, coherent anti-Stokes Raman scattering (CARS) microscopy [3] based on four-wave mixing (FWM) can provide molecular-specific image contrast reflecting vibrational resonances with high sensitivity. Indeed, high-speed vibrational imaging at up to the video rate was demonstrated [6]. In biological applications, however, it is crucial to suppress so-called nonresonant signals emitted from solvent, which significantly reduce the contrast of resonant CARS signals of interest. Although various approaches have been proposed to suppress nonresonant signals [7-11], they typically suffer from signal loss and/or increased complexity of the setup.

Stimulated Raman scattering (SRS) is another well-known nonlinear Raman phenomenon in which photon energy is transferred from an anti-Stokes (AS) pulse to a Stokes (S) pulse when the frequency difference matches a Raman vibrational mode [12]. SRS reflects only vibrational resonances and is unsusceptible to nonresonant nonlinearities, providing us with high vibrational contrast. Taking advantage of this fact, the application of SRS to vibrational microscopy has been recently reported by several groups [13-16]. An important issue of SRS microscopy is its sensitivity, which was thought to be much lower than that of CARS because the SRS signal is detected as a small change of the intensity of excitation beam, and hence is deteriorated by shot noise and laser intensity noise. Indeed, an early demonstration [14] used amplified femtosecond pulse trains at low repetition rate for excitation, which may cause damages to biological samples. Thereafter, our group and Freudiger *et al.* independently demonstrated biological imaging by SRS microscopy using a quiet mode-locked laser for excitation [15, 16]. The SRS microscopy is shown to have higher sensitivity than spontaneous Raman scattering microscopy and to be able to incorporate a laser-scanning mechanism and forward- and epi-detection geometries [16]. Furthermore, we pointed out in Ref. 15 that the shot-noise-limited sensitivity of SRS microscopy is comparable to that of CARS microscopy because SRS can be viewed as the homodyne detection of the nonlinear-optical signal with the excitation pulse. Although this prediction would further enhance the merit of SRS microscopy, its actual sensitivity has yet to be investigated.

In this paper, we present a detailed analysis on the sensitivity of SRS microscopy, and experimentally demonstrate that the sensitivity of our SRS microscope is lower than the theoretical limit only by <15 dB, quantitatively supporting the high sensitivity of SRS microscopy. We also present results of live-cell imaging with SRS microscopy.

2. Theory of SRS microscopy

In SRS microscopy, AS and S pulses at angular frequencies of ω_1 and ω_2 ($\omega_1 > \omega_2$) are focused into a sample, and the intensity change of the AS pulse due to SRS is detected. Intuitively, SRS is caused by the optical phase modulation induced by the time-dependent refractive index reflecting the molecular vibration, which is coherently driven by the intensity beat between AS and S pulses [12]. In order to detect the small intensity change of AS pulse, the S pulse is intensity-modulated in time, and the SRS signal is obtained through the lock-in detection of the intensity of the AS pulse collected.

#106468 - $15.00 USD Received 16 Jan 2009; revised 21 Feb 2009; accepted 21 Feb 2009; published 24 Feb 2009

Here, we derive an expression of the sensitivity of SRS to compare it with that of CARS. The analysis is based on a classical calculation, which quantitatively agrees with the quantum-mechanical one in typical situations of SRS microscopy, where the light-matter interaction is so weak that we can neglect the effect of saturation of molecular vibration and that of the spontaneous emission, which is overwhelmed by the shot noise of the excitation pulse. If we denote the complex electric fields of the excitation pulses at ω_1 and ω_2 by E_1 and E_2, respectively, third-order nonlinear polarizations at ω_1 and $2\omega_1 - \omega_2$ (i.e. FWM) can be expressed as [12]

$$P_1 = 3\varepsilon_0(2\chi_e + \chi_R)E_1|E_2|^2, \tag{1}$$

$$P_{FWM} = 3\varepsilon_0(\chi_e + \chi_R)E_1^2E_2^*, \tag{2}$$

where ε_0 is the vacuum permittivity, and χ_e and χ_R are electronic and vibrational third-order nonlinear susceptivities, respectively. If there is no electronic transition resonance at ω_1, ω_2, $2\omega_1$ and $2\omega_2$ (i.e. samples are transparent around the wavelength of excitation pulses), electronic nonlinear process is nonresonant and hence χ_e is real. χ_R is a function of $\omega_1 - \omega_2$, and Im χ_R corresponds to vibrational resonances. These polarizations drive electric fields, which are given by

$$\Delta E_1 = \frac{i\omega_1 P_1 l}{2n\varepsilon_0 c} = \frac{3i\omega_1 l}{2nc}(2\chi_e + \chi_R)E_1\left|E_2\right|^2 = i\gamma\omega_1(2\chi_e + \chi_R)E_1\left|E_2\right|^2, \tag{3}$$

$$\Delta E_{FWM} = \frac{i\omega_{FWM} P_{FWM} l}{2n\varepsilon_0 c} = \frac{3i\omega_{FWM} l}{2nc}(\chi_e + \chi_R)E_1^2E_2^* = i\gamma\omega_{FWM}(\chi_e + \chi_R)E_1^2E_2^*, \tag{4}$$

where n is the refractive index, c is the speed of light, l is the effective interaction length at the focus and $\gamma \equiv 3l/2nc$ is a proportional constant. For simplicity, we assumed that the refractive index is almost the same at ω_1 and ω_{FWM}. We also neglected the effect of the phase matching condition in Eq. (4), which is almost satisfied under tight focusing conditions. The terms $i\omega$ in Eqs. (3) and (4) originate from the fact that, in the time domain, the electric fields are driven by the derivative of polarizations with respect to the time [17]. These fields are added to the incident fields. Since the origin of SRS is the interference between ΔE_1 and E_1, SRS can be viewed as the homodyne detection of ΔE_1 with E_1. The phase sensitivity of homodyne allows the discrimination between resonant and nonresonant nonlinearities, as will be shown below.

From Eq. (3) and (4), we can derive the numbers of signal photons S of SRS and FWM. As for FWM,

$$S_{FWM} = \frac{2\varepsilon}{\hbar\omega_{FWM}}\left|\Delta E_{FWM}\right|^2 A_{eff}\frac{cT}{n} = \frac{\Gamma}{\omega_{FWM}}\left|\Delta E_{FWM}\right|^2 = \Gamma\gamma^2\omega_{FWM}\left|\chi_e + \chi_R\right|^2\left|E_1\right|^4\left|E_2\right|^2, \tag{5}$$

where ε is the permittivity, $\hbar\omega_{FWM}$ is the photon energy, A_{eff} is the effective area of the focus, T is the effective exposure time and $\Gamma \equiv 2\varepsilon A_{eff}cT/\hbar n$ is a proportional constant. T is expressed as

$$T = \Delta t\, f_{rep}\tau, \tag{6}$$

where Δt is the pulse width, f_{rep} is the repetition frequency, and τ is the pixel dwell time. Considering the Poisson distribution of photons, the shot noise of the FWM signal photons is given by

$$N_{FWM} = \sqrt{S_{FWM}}\,. \tag{7}$$

If we define the contrast of CARS signal as

#106468 - $15.00 USD Received 16 Jan 2009; revised 21 Feb 2009; accepted 21 Feb 2009; published 24 Feb 2009

$$V = \frac{\left|\chi_e + \chi_R\right|^2 - \left|\mathrm{Re}(\chi_e + \chi_R)\right|^2}{\left|\chi_e + \chi_R\right|^2} = \frac{\left|\mathrm{Im}\,\chi_R\right|^2}{\left|\chi_e + \chi_R\right|^2}, \tag{8}$$

the shot-noise-limited signal-to-noise ratio (SNR) is given by

$$\mathrm{SNR}_{\mathrm{CARS}} = \left(\frac{S_{\mathrm{FWM}} V}{N_{\mathrm{FWM}}}\right)^2 = \Gamma\gamma^2\omega_{\mathrm{FWM}} \frac{\left|\mathrm{Im}\,\chi_R\right|^4}{\left|\chi_e + \chi_R\right|^2} \left|E_1\right|^4 \left|E_2\right|^2. \tag{9}$$

On the other hand, the number of photons of SRS is given by

$$\begin{aligned} S_{\mathrm{SRS}} &= \frac{\Gamma}{\omega_1}\left(\frac{1}{2}\left|E_1\right|^2 - \frac{1}{2}\left|E_1 + \Delta E_1\right|^2\right) \\ &= \Gamma\gamma\,\mathrm{Im}\,\chi_R \left|E_1\right|^2 \left|E_2\right|^2, \end{aligned} \tag{10}$$

where we assumed $|\Delta E_1| << |E_1|$ and the factor of 1/2 accounts for the fact that SRS is detected through the lock-in detection, in which SRS process occurs only when the S pulse is turned on. The shot noise is given by

$$N_{\mathrm{SRS}} = \sqrt{\frac{\Gamma \mid E_1 \mid^2}{\omega_1}}. \tag{11}$$

From Eqs. (10) and (11), we obtain

$$\mathrm{SNR}_{\mathrm{SRS}} = \left(\frac{S_{\mathrm{SRS}}}{N_{\mathrm{SRS}}}\right)^2 = \Gamma\gamma^2\omega_1 \left|\mathrm{Im}\,\chi_R\right|^2 \left|E_1\right|^2 \left|E_2\right|^4. \tag{12}$$

where SNR is defined as the energy ratio of signal to noise of the detected photocurrent. By using Eqs. (9) and (12), we can calculate the ratio of the shot-noise-limited SNR's as

$$\frac{\mathrm{SNR}_{\mathrm{SRS}}}{\mathrm{SNR}_{\mathrm{CARS}}} = \frac{\omega_1}{\omega_{\mathrm{FWM}}} \frac{\left|\chi_e + \chi_R\right|^2}{\left|\mathrm{Im}\,\chi_R\right|^2} \frac{\left|E_2\right|^2}{\left|E_1\right|^2}, \tag{13}$$

which is on the order of 1. Eq. (13) can be higher than 1 especially when the nonresonant nonlinearity is much larger than resonant nonlinearity (i.e. $|\chi_e + \chi_R| >> |\mathrm{Im}\ \chi_R|$). In that case, however, the sensitivity of CARS can be improved to some extent by taking advantage of the interference between χ_e and χ_R at off-resonance. Anyway, Eq. (13) indicates that the shot-noise limited sensitivity of SRS is comparable to CARS.

Intuitively, the similarity of the SNR's can be understood as follows. Shot noise of light in the coherent state is equivalent to the optical beat between the electric field and the vacuum fluctuation. Thus, in the shot-noise limit, the SNR is determined mainly by the ratio of the signal field (i.e. Eqs. (3) and (4)) to the vacuum fluctuation, which is almost the same for SRS and CARS.

In SRS microscopy, we can easily compare the actual sensitivity with the shot-noise-limited one. This is because the shot-noise in the lock-in voltage v_{shot} can be calculated from the detector current I by using the relationship

$$v_{\mathrm{shot}} = \sqrt{\frac{2Ie}{\tau}} GZ, \tag{14}$$

where $e = 1.6 \times 10^{-19}$ C is the elementary charge, G is the gain of electric circuits, and Z is the transimpedance of the photodetection circuit. The factor of $2^{1/2}$ accounts for the fact that typical lock-in amplifiers output the amplitude of the input signal instead of the root-mean-

#106468 - $15.00 USD Received 16 Jan 2009; revised 21 Feb 2009; accepted 21 Feb 2009; published 24 Feb 2009

squared voltage. In the derivation of Eq. (14), we assumed that the electric power of the shot noise in an RF signal is equal to that after lock-in detection. This is because the former and the latter have noise bandwidths of τ^{-1} and $\tau^{-1}/2$, respectively, whereas the half of the noise in the former is in the quadrature phase and disappears after the down-conversion.

Note that Eq. (13) neglects various effects such as efficiency and thermal noise of the detector, and intensity noise of laser pulses. Among them, the intensity noise is quite important to take into account in SRS microscopy because it can easily surpass the shot noise. Therefore, to achieve a high sensitivity, we should employ a quiet laser source such as a mode-locked laser and/or suitable equipment for suppressing intensity noise such as an intensity stabilizer based on a feedback or feed-forward circuit. Moreover, it is preferable to increase the frequencies of modulation and lock-in detection because the relative intensity noise of laser pulses typically decreases with frequency owing to the intensity averaging effect, which is caused by the finite relaxation time of the gain medium. Furthermore, the use of high-repetition rate laser seems attractive not only for increasing the modulation frequency but also for increasing the acquisition rate. As for the efficiency of the detector, SRS is advantageous because we can use an ordinary silicon photodiode (PD), which is cheap and has a high efficiency of >90 %. The thermal noise can be negligible compared to the shot noise when the optical power is higher than several milliwats and detector circuits are properly designed.

3. Experiment

We experimentally investigated the actual sensitivity of our SRS microscope by using the setup shown in Fig. 1. A Ti:sapphire laser (Coherent, Mira 900F) generated AS pulses with a pulse duration of approximately 100 fs at a wavelength of 767 nm. An optical parametric oscillator (OPO) (Coherent, Mira OPO) generated S pulses with a duration of approximately 200 fs at a wavelength of around 1000 nm. The repetition rate of the pulses was 76 MHz. An acousto-optic modulator (AOM) (Brimrose, TEM-200-50-1000) was placed for the intensity modulation of the S pulses at a modulation frequency of 10.7 MHz. The modulation depth of AOM was >70 %. These pulses were collinearly combined with a dichroic mirror and focused inside a sample by an oil-immersion objective lens (Olympus, UPLSAPO 100XO) with a numerical aperture (NA) of 1.4. The sample position was scanned by a piezoelectric transducer stage (Physik Instrumente, P-611.3S). The output pulses from the sample were collected by another lens with the same NA. After S pulses are removed by an optical filter, AS pulses are detected by a silicon PD (Hamamatsu, S5821-01). Its photocurrent was measured by a home-made transimpedance amplifier, band-pass filtered by a ceramic filter, downconverted to 100 kHz by an RF mixer and measured by a lock-in amplifier (LIA) (NF Corp., LI5640). The time constant of the LIA was set to <0.3 ms with a slope of 24 dB/oct. The lock-in signal is measured by a personal computer equipped with an analog-to-digital converter and is averaged over a pixel dwell time.

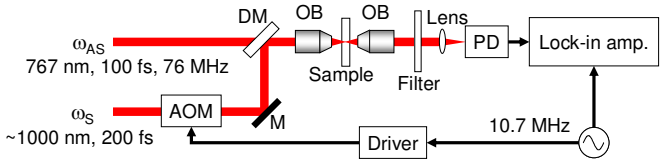

Fig. 1. Experimental setup of SRS microscopy. DM: dichroic mirror. OB: objective lens. PD: photodiode. AOM: acousto-optic modulator.

Figure 2(a) shows the dependences of the SRS signal on the Raman shift ($\omega_{AS} - \omega_S$). As a sample, we used polystyrene beads with a diameter of 4.5 μm in water. The Raman shift was scanned from 2950 to 3600 cm^{-1}. This scan range was limited by the specification of our OPO. As shown in Fig. 2(a), SRS signal was maximized at around 3090 cm^{-1}, showing that the aromatic CH stretching mode at 3054 cm^{-1} is successfully detected. We attributed the discrepancy between the Raman frequencies to the insufficient calibration of our spectrometer.

#106468 - $15.00 USD Received 16 Jan 2009; revised 21 Feb 2009; accepted 21 Feb 2009; published 24 Feb 2009

The Raman spectrum is broadened because we used femtosecond pulses instead of picosecond ones for excitation. Figure 2(b) shows the dependence of the SRS signal on the excitation powers of AS and S pulses, which are denoted by P_{AS} or P_S, respectively. The power of one of the pulses is changed while the other is fixed at 0.2 mW. We can see that the SRS signal is proportional to the product of P_S and P_{AS}, which agrees with Eq. (10).

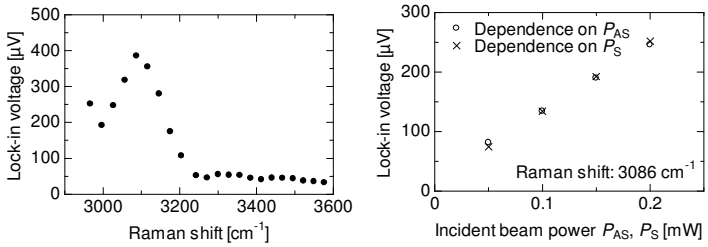

Fig. 2. (a) SRS spectrum of a polystyrene bead. (b) Dependence of SRS signal on the excitation beam powers. Raman shift: 3086 cm^{-1}.

To investigate the sensitivity of the SRS microscope, we measured the noise levels of our setup. When only AS pulses were impinged on the PD and S pulses were blocked, the noise level of the lock-in signal was measured to be v_N = 12.8 μV. The shot-noise level was calculated by Eq. (14) to be v_{shot} = 2.5 μV using I = 0.25 mA, τ = 5 ms, G = 18, and Z = 1.1 kΩ. The noise level of the electric circuits v_c was measured to be 6.9 μV. The noise level due to the laser intensity noise was evaluated to be

$$v_L = (v_N^2 - v_{shot}^2 - v_c^2)^{1/2} = 10.5\ \mu V. \quad (15)$$

Thus the noise in the current setup is dominated by the intensity noise. Nevertheless, the current setup has a sensitivity that is lower than the theoretical limit only by v_N/v_{shot} = 14.2 dB, proving the high sensitivity of SRS microscopy. In this way, the high-frequency intensity noise of the AS pulses is sufficiently small to take advantage of SRS in terms of sensitivity and contrast.

Figure 3(a) shows the SRS image of the polystyrene bead. The Raman shift was set to 2967 cm^{-1}. P_{AS} and P_S were set to 0.4 mW and 0.2 mW, respectively. For comparison, we also acquired a CARS image using another set of optical filters and a photomultiplier tube. Figures 3(a)(b) compare the SRS and CARS images. In the SRS image, the water doesn't emit any signal, leading to a high contrast. In turn, the CARS image is accompanied by a large amount of non-resonant background from water. These characteristics are clearly presented in one-dimensional cross sections shown in Fig. 3(c). The SNR's of SRS and CARS signals from polystyrene were almost the same and were >20 dB. Note that the contrasts of SRS and CARS can be further improved by using picosecond pulses instead of femtosecond ones.

#106468 - $15.00 USD Received 16 Jan 2009; revised 21 Feb 2009; accepted 21 Feb 2009; published 24 Feb 2009

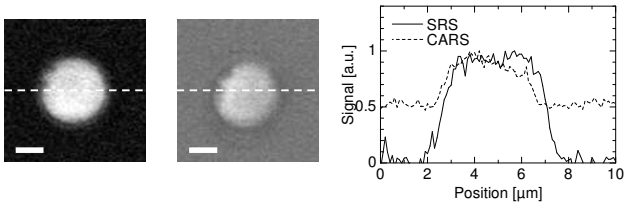

Fig. 3. Images of a polystyrene bead with (a) SRS and (b) CARS. The diameter of the bead: 4.5 μm. Pixel dwell time: 2 ms. Scale bar: 2 μm. Number of pixels: 100 × 100. (c) Cross-sections at the broken lines in (a) and (b).

SRS microscopy is readily applicable to the observation of unstained live-cells. Considering that the lock-in signal is proportional to Im χ_R, we constructed images in such a way that the image intensity is proportional to $(\mathrm{Im}\ \chi_R)^2$. The Raman shift was set to 2967 cm^{-1}. P_{AS} and P_S were set to 0.8 mW and 0.2 mW, respectively. As shown in Figs. 4(a) and 4(b), the nucleus and cell walls of a tobacco BY-2 cultured cell are clearly visualized in 2D and 3D, respectively, based on vibrational contrast by CH stretching modes. We feel that the 3D SRS image is accompanied by smaller amounts of artifacts in the deep region. This is probably due to the fact that the phase matching condition of SRS is automatically satisfied. This point should be investigated in future.

Finally, the transverse and axial resolutions were measured by observing a polystyrene bead with a diameter of 0.05 μm. As shown in Fig. 5, they were found to be 0.48 μm and 1.1 μm, respectively. A slight amount of offset may be caused by cross-phase modulation effect [5] which comes from Re $\chi^{(3)}$, and could be reduced by using picosecond pulses.

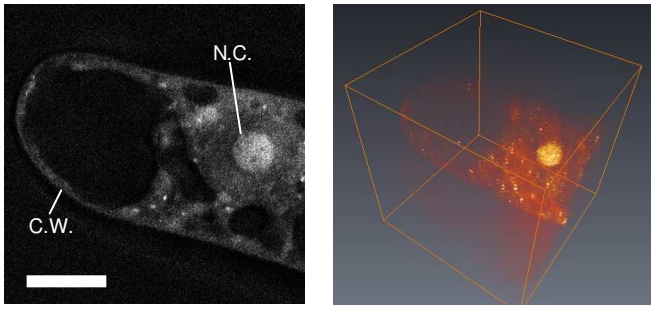

Fig. 4. SRS images of an unstained tobacco BY-2 cell. Pixel dwell time: 3 ms. (a) 2D image. Number of pixels: 400 × 400. C.W.: cell wall. N.C.: nucleus. Scale bar: 10 μm. (b) 3D image. Volume size: 40 × 40 × 40 μm^3. Number of pixels: 160 × 160 × 40.

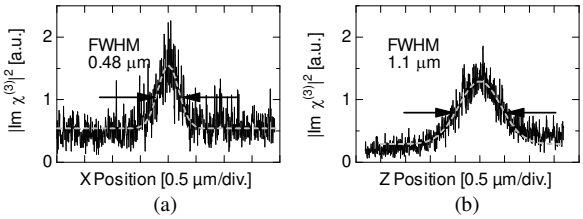

Fig. 5. Cross-sectional curves of SRS signal of a polystyrene bead with a diameter of 50 nm. (a) Lateral direction. (b) Axial direction. Pixel dwell time: 10 ms.

#106468 - $15.00 USD Received 16 Jan 2009; revised 21 Feb 2009; accepted 21 Feb 2009; published 24 Feb 2009

It should be noted that our SRS microscope is extremely tolerant of stray light because its effect on the photocurrent is buried in the shot noise of AS pulse. In spite of the fact that our home-made PD circuit is equipped in a metal case and stray light can be incident on the PD, we didn't confirm any degradation of SNR of SRS signal even under the room light. On the other hand, the photomultiplier used for the detection of CARS signals was highly susceptible to the room light and careful removal of stray light was crucial. Furthermore, the rejection ratio of optical filters used in SRS microscopy is much lower than those used in CARS, permitting us to decrease the insertion loss of the filters. These are additional advantages of SRS from a practical viewpoint.

4. Summary

We have presented the theory of sensitivity of SRS microscopy to show that, in the shot-noise limit, SRS can have a high sensitivity that is comparable to CARS. We experimentally demonstrated that the sensitivity of our SRS microscope readily has a high sensitivity that is lower than the shot noise limit by <15 dB owing to the low-noise nature of mode-locked lasers. The presented results quantitatively validate the high-sensitivity nature of SRS microscopy, and enhance the attractive features of SRS microscopy such as high contrast and high tolerance for stray light.

Acknowledgments

This research is supported by a Grant-in-Aid for Scientific Research (B) (No. 20360033) from Japan Society for the Promotion of Science. Y. O. is supported by a Grant-in-Aid for Young Scientists (B) (No. 20760036) from the Ministry of Education, Culture, Sports, Science, and Technology of Japan. This work was also supported in part by SENTAN, JST (Japan Science and Technology Agency).

#106468 - $15.00 USD Received 16 Jan 2009; revised 21 Feb 2009; accepted 21 Feb 2009; published 24 Feb 2009